Robotics: Science and Systems 2016
Ann Arbor, MI, USA, June 18-22, 2016

Probabilistic Approaches to the $AXB = YCZ$ Calibration Problem in Multi-Robot Systems

Qianli Ma, Zachariah Goh, Gregory S. Chirikjian
Department of Mechanical Engineering
Johns Hopkins University
Baltimore, Maryland 21218
Email: {mqianli1, zach.goh, gchirik1}@jhu.edu

Abstract*—In recent years, the topic of multi-robot systems has become very popular. These systems have been demonstrated in various applications, including exploration, construction, and warehouse operations. In order for the whole system to function properly, sensor calibrations such as determining the camera frame relative to the IMU frame are important. Compared to the traditional hand-eye & robot-world calibration, a relatively new problem called the $AXB = YCZ$ calibration problem arises in the multi-robot scenario, where A, B, C are rigid body transformations measured from sensors and X, Y, Z are unknown transformations to be calibrated. Several solvers have been proposed previously in different application areas that can solve for X, Y and Z simultaneously. However, all of the solvers assume a priori knowledge of the exact correspondence among the data streams $\{A_i\}$, $\{B_i\}$ and $\{C_i\}$. While that assumption may be justified in some scenarios, in the application domain of multi-robot systems, which may use ad hoc and asynchronous communication protocols, knowledge of this correspondence generally cannot be assumed. Moreover, the existing methods in the literature require good initial estimates that are not always easy or possible to obtain. In this paper, we propose two probabilistic approaches that can solve the $AXB = YCZ$ problem without a priori knowledge of the correspondence of the data. In addition, no initial estimates are required for recovering X, Y and Z. These methods are particularly well suited for multi-robot systems, and also apply to other areas of robotics in which $AXB = YCZ$ arises.

I. INTRODUCTION

Many multirobot calibration problems can be formulated using the equation $AXB = YCZ$, where A, B and C are known homogeneous transformations from sensor readings, and X, Y and Z are unknown relationships between two target frames. For the dual arm system [20] shown in Fig. (1), the problem becomes the hand-eye (X), robot-robot (Y) and tool-flange (Z) calibration problem where robot 1 holds the camera and robot 2 holds the marker. For a team of mobile robots [8] illustrated in Fig. (2), a triple hand-eye (or camera-marker) calibration problem exists where each robot agent is "looking at" the marker on the next agent. In Fig. (3), the problem of the serial-parallel hybrid robot system [23] is cast as the tool-gripper (X), flange-base (Y) and camera-base (Z) calibrations. The same mathematical modeling also exists in co-robotic ultrasound (US) tomography where two hand-eye and one robot-robot calibrations are needed [1]. However, relatively little work has been done on $AXB = YCZ$ calibration. To the best of our knowledge, only Wang [20, 22] and Yan [23] proposed several algorithms for solving X, Y and Z simultaneously.

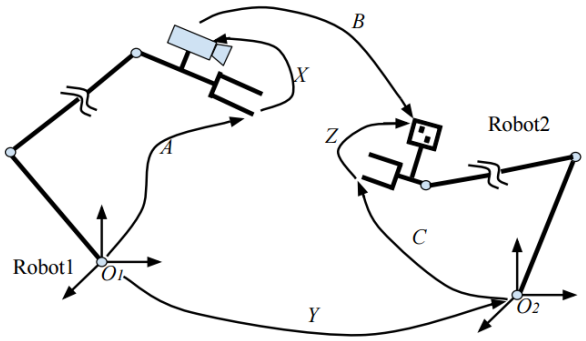

Fig. 1: The Hand-Eye, Robot-Robot, Tool-Flange Calibration of a Dual Arm System

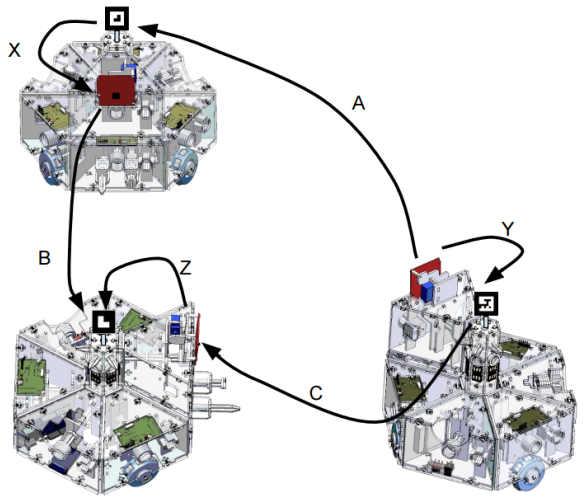

Fig. 2: Triple Hand-Eye Calibration of a Multi-Robot System

A. RELATED WORK

The $AXB = YCZ$ problem first originated as an extension of the robot hand-eye problem. The hand-eye calibration problem can be formulated as $AX = XB$, where A and B are homogeneous transformations calculated from sensor

readings, and X is the unknown transformation from the mounted sensor (US probe, camera, etc.) to the robot end-effector. Tsai [19] and Shiu [18] were among the first to solve the $AX = XB$ problem. Many other solvers have also been proposed in the literature [2, 3, 4, 7, 10, 13, 16, 24]. The hand-eye and robot-world calibration problem is an extension of the hand-eye problem, and is formulated as $AX = YB$ where X denotes the transformation between sensor and the end-effector and Y describes the transformation between the robot base frame and the world frame. In this formulation, A and B are the homogeneous transformations measured directly from sensors. Quite a few $AX = YB$ solvers have been proposed in the literature [9, 11, 12, 14, 15, 17, 25]. Most of the existing $AX = XB$ and $AX = YB$ solvers deal with the case where there is an exact correspondence between the data pairs A_i and B_i. However, this is generally not true in real applications due to asynchronous sensors or missing data. [2] and [15] proposed probabilistic approaches for solving the $AX = XB$ and $AX = YB$ problems respectively, and both of them show the superiority of the probabilistic approaches over the traditional solvers when handling data without a priori knowledge of correspondence.

B. CONTRIBUTIONS

In this paper, we propose two "probabilistic" frameworks for solving the $AXB = YCZ$ robot system calibration problem. Due to the different physical properties of the robotic system, two types of probabilistic $AXB = YCZ$ solvers exist which greatly reduce the need for a priori knowledge of the correspondence between sensor data. We use the word "probabilistic" because the measured datasets $\{A_i\}$, $\{B_i\}$, and $\{C_i\}$ are each replaced with histograms on the space of rigid-body poses, and normalized to be probability densities. That is, while there are no random variables in this problem, the tools of probability and measure theory can still be employed with great benefit.

The rest of the paper is organized as follows. In section II, we introduce some of the fundamental mathematical background. Section III describes in detail the formulation of the two probabilistic $AXB = YCZ$ solvers. In section IV, we perform numerical simulations to compare the probabilistic and traditional $AXB = YCZ$ solvers, and show the effectiveness and robustness of the former. Comparison between the two probabilistic approaches are also performed to show their respective desired application scenario. In section V, we draw conclusions and point out future directions.

II. MATHEMATICAL BACKGROUND

Before going into the probabilistic solvers for the $AXB = YCZ$ problem, we provide a brief introduction to the concepts of mean, covariance and convolution on the special Euclidean group $SE(3)$.

The special Euclidean group $SE(3)$ is the space consisting of rigid body transformations of the following form:

$$H(R,t) = \begin{pmatrix} R & t \\ 0^T & 1 \end{pmatrix} \in SE(3), \quad R \in SO(3) \tag{1}$$

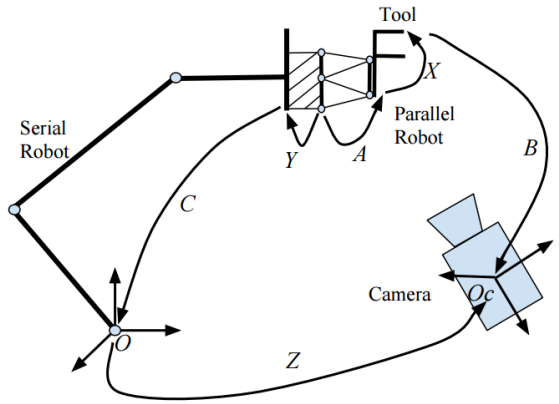

Fig. 3: Flange-Base, Camera-Base and Tool-Gripper Calibration of a Serial-Parallel Manipulator

where $t \in \mathbb{R}^3$ is a translation vector and $SO(3)$ denotes the special orthogonal group consisting of 3×3 rotation matrices. T denotes the transpose of a vector or matrix and H is the symbol for a group element in $SE(3)$. The group operation is matrix multiplication.

There is a unique and correct way to define integration on $SE(3)$ called the "Haar measure", and is denoted as dH. In particular, if R is expressed in ZXZ Euler angles (α, β, γ), then to within an arbitrary scale factor $dH = \sin\beta \, d\alpha \, d\beta \, d\gamma \, dt_1 \, dt_2 \, dt_3$. Within this context, the convolution of two well-behaved functions can be defined as [5, 6]:

$$(f_1 * f_2)(H) = \int_{SE(3)} f_1(K) f_2(K^{-1}H) \, dK \tag{2}$$

where $K, H \in SE(3)$. The integral over $SE(3)$ can be expressed in various coordinates and here we choose the exponential coordinates, where the six-dimensional integral over $SE(3)$ and its measure can be found in [21].

As it will be used in later sections, we define a Dirac delta function on $SE(3)$, $\delta(H)$, by the properties

$$(f * \delta)(H) = \int_{SE(3)} f(K)\delta(K^{-1}H) \, dK = f(H), \tag{3}$$

and

$$\int_{SE(3)} \delta(H) dH = 1. \tag{4}$$

Informally, we can think of $\delta(H)$ as an infinite spike of the form

$$\delta(H) = \begin{cases} +\infty & \text{if} \quad H = \mathbb{I}_4 \\ 0 & \text{if} \quad H \neq \mathbb{I}_4 \end{cases} \tag{5}$$

where $\delta(H)$ is only nonzero at the identity and zero elsewhere, $H \in SE(3)$ and $\mathbb{I}_4$ denotes a 4 by 4 identity matrix. Given $A \in SE(3)$, the corresponding shifted version of the Dirac delta function can be defined as $\delta_A(H) = \delta(A^{-1}H)$.

In the probabilistic approaches to be introduced, all $SE(3)$ elements will be represented by their mean M and covariance Σ. Given a probability density function (PDF) as $f(H)$, its

mean and covariance are defined to satisfy the following equations [5, 21]:

$$\int_{SE(3)} \log(M^{-1}H) f(H)\, dH = \mathbb{O}_4 \tag{6a}$$

$$\Sigma = \int_{SE(3)} \log^{\vee}(M^{-1}H)[\log^{\vee}(M^{-1}H)]^T f(H)\, dH \tag{6b}$$

where $\mathbb{O}_4$ denotes the 4×4 zero matrix and $H = \exp \widehat{\mathbf{h}}$, $\widehat{\mathbf{h}} \in se(3)$, $\mathbf{h} = \log^{\vee}(H) \in \mathbb{R}^6$, and

$$\log(H) = \begin{pmatrix} 0 & -h_3 & h_2 & h_4 \\ h_3 & 0 & -h_1 & h_5 \\ -h_2 & h_1 & 0 & h_6 \\ 0 & 0 & 0 & 0 \end{pmatrix}. \tag{7}$$

Given a PDF describing $\{A_i\}$ as $f_A(H)$, where $i = 1, \ldots, n$, the corresponding discrete versions of the mean and covariance are:

$$\sum_{i=1}^{n} \log(M_A^{-1} A_i) = \mathbb{O}_4 \tag{8a}$$

$$\Sigma_A = \sum_{i=1}^{n} \log^{\vee}(M_A^{-1} A_i)[\log^{\vee}(M_A^{-1} A_i)]^T. \tag{8b}$$

Numerically, given a set of A_i, M_A can be solved in an iterative manner as described in [21]. In the context of $AXB = YCZ$ calibration, M_B and M_C can be computed in a similar fashion, and Σ_A, Σ_B and Σ_C are straightforward to compute given M_A, M_B and M_C. Given two PDFs f_1 and f_2 on $SE(3)$, if both of them are "highly-focused" in the sense that $\|\Sigma_1\| \ll 1$ and $\|\Sigma_2\| \ll 1$, then the mean and covariance of their convolution $(f_1 * f_2)(g)$ can be calculated as [21]:

$$M_{1*2} = M_1 M_2 \tag{9a}$$

$$\Sigma_{1*2} = Ad(M_2^{-1})\Sigma_1 Ad^T(M_2^{-1}) + \Sigma_2 \tag{9b}$$

where

$$Ad(H) = \begin{pmatrix} R & \mathbb{O}_3 \\ \hat{t}R & R \end{pmatrix}. \tag{10}$$

The "hat" operation here converts a three dimensional vector into a skew-symmetric matrix:

$$\hat{t} = \begin{pmatrix} 0 & -t_3 & t_2 \\ t_3 & 0 & -t_1 \\ -t_2 & t_1 & 0 \end{pmatrix}. \tag{11}$$

The following is also true and will be used later:

$$Ad(H^{-1}) = Ad^{-1}(H) = \begin{pmatrix} R^T & \mathbb{O} \\ -\widehat{R^T t} R^T & R^T \end{pmatrix}. \tag{12}$$

III. Problem Formulation

In this section, we derive the mathematical frameworks of the two probabilistic approaches for the $AXB = YCZ$ problem. They share a common theoretical framework but are designed for different types of robotic systems.

A. Fundamental Framework

Given a large set of triples $(A_i, B_i, C_i) \in SE(3) \times SE(3) \times SE(3)$ where $i = 1, \cdots, n$, the following equation can be obtained:

$$A_i X B_i = Y C_i Z. \tag{13}$$

Using the shifting property of Dirac delta function, we have

$$(\delta_{A_i} * \delta_X * \delta_{B_i})(H) = \delta(B_i^{-1} X^{-1} A_i^{-1} H) \tag{14a}$$

$$(\delta_Y * \delta_{C_i} * \delta_Z)(H) = \delta(Z^{-1} C_i^{-1} Y^{-1} H). \tag{14b}$$

Using Eq. (5) and Eq. (13), the above two equations can be combined into a single equation as:

$$(\delta_{A_i} * \delta_X * \delta_{B_i})(H) = (\delta_Y * \delta_{C_i} * \delta_Z)(H). \tag{15}$$

Next, define the PDF of $\{G_i\}$ as:

$$f_G(H) = \frac{1}{n} \sum_{i=1}^{n} \delta_{G_i}(H) \tag{16}$$

where $G \in \{A, B, C\}$. Then use the bi-linearity of convolution, add n instances of Eq. (15), substitute Eq. (16) into the summation, and if we further constrain f_A, f_B and f_C to be highly focused, we get:

$$(f_A * \delta_X * f_B)(H) \approx (\delta_Y * f_C * \delta_Z)(H). \tag{17}$$

Unlike in the $AX = XB$ and $AX = YB$ problems in which similar steps were used in [2, 15] to produce exact results, in the $AXB = YCZ$ problem the step from Eq. (15) to Eq. (17) is an approximation. This is because the left-hand side of Eq. (15) couples A_i and B_i, whereas in Eq. (17) the sets A and B are treated as independent. This approximation is justified by the smallness of the products of the covariances of A and B, which follows from the assumption that the distributions are highly focused. Then by employing Eq. (9a) twice, we get the mean equation of $AXB = YCZ$ as

$$M_A M_X M_B \approx M_Y M_C M_Z. \tag{18}$$

Because X, Y and Z are all single elements of $SE(3)$, $M_X = X$, $M_Y = Y$, $M_Z = Z$, and $\Sigma_X = \mathbb{O}$, $\Sigma_Y = \mathbb{O}$, $\Sigma_Z = \mathbb{O}$. Eq. (18) then becomes

$$\boxed{M_A X M_B \approx Y M_C Z} \tag{19}$$

The covariance equation is obtained by first computing Σ_{A*X} and then Σ_{A*X*B} as:

$$\Sigma_{A*X*B} = Ad(B^{-1})Ad(X^{-1})\Sigma_A Ad^T(X^{-1})Ad^T(B^{-1}) + \Sigma_B \tag{20}$$

Similarly, Σ_{Y*C*Z} can be obtained as:

$$\Sigma_{Y*C*Z} = Ad(Z^{-1})\Sigma_C Ad^T(Z^{-1}) \tag{21}$$

Therefore, by equating Eq. (20) and Eq. (21), the covariance equation for $AXB = YCZ$ becomes

$$\boxed{\begin{array}{c} Ad(B^{-1})Ad(X^{-1})\Sigma_A Ad^T(X^{-1})Ad^T(B^{-1}) + \Sigma_B \approx \\ Ad(Z^{-1})\Sigma_C Ad^T(Z^{-1}) \end{array}} \tag{22}$$

To simplify notation, we will treat subsequent approximations as equalities. In order to decompose Eq. (22) into subequations, define the covariance matrix as

$$\Sigma_H = \begin{pmatrix} \Sigma_H^1 & \Sigma_H^2 \\ \Sigma_H^3 & \Sigma_H^4 \end{pmatrix} \in \mathbb{R}^{6\times 6} \tag{23}$$

where $H = A, B, C$ and $\Sigma_H^i \in \mathbb{R}^{3\times 3}$. To simplify the notation, we define $U = \hat{t}$. Substitute Eq. (23) into Eq. (22) and one gets the upper left block as

$$R_B^T R_X^T \Sigma_A^1 R_X R_B + \Sigma_B^1 = R_Z^T \Sigma_C^1 R_Z, \tag{24}$$

and the lower right block as

$$\begin{array}{c} R_B^T R_X^T \Sigma_A^1 W_{XB}^T + R_B^T R_X^T \Sigma_A^2 R_X R_B + \Sigma_B^2 = \\ R_Z^T \Sigma_C^1 R_Z U_Z^T + R_Z^T \Sigma_C^2 R_Z \end{array} \tag{25}$$

where $W_{XB} := U_B R_B^T R_X^T + R_B^T U_X R_X^T$. For convenience, we call Eq. (24) the Sig-Rot equation and Eq. (25) the Sig-Trans equation. Sig-Rot equation contains only the rotational information from the unknown matrices while Sig-Trans equation contains both the rotational and translational information. These two equations are not sufficient to solve the problem since Eq. (24) contains only R_X and R_Z, and Eq. (25) contains only t_X and t_Z in addition to the above two rotations, whereas Y is "lost" in the covariance equation. However, it turns out that by rearranging the order of X, Y and Z, similar equations to Eq. (24) and Eq. (25) can be obtained to solve for the unknown transformations.

There are a total of six variations of $AXB = YCZ$ formulations. If we write $AXB = YCZ$ as $AXBZ^{-1}C^{-1}Y^{-1} = \mathbb{I}$ and premultiply by A^{-1} and postmultiply by A on both sides of the equation, we have $XBZ^{-1}C^{-1}Y^{-1}A = \mathbb{I}$ which "moves" A from the left to the right. The same operation can be done in turn for X, B, Z^{-1}, C^{-1} and Y^{-1} and these give a total of six variations, which can be converted back into the $AXB = YCZ$ form as shown in the "Representation" column of Table I .

For most $AX = XB$ and $AX = YB$ calibration solvers, a common approach is to solve for rotations first and then the solution of translations becomes easier. The $AXB = YCZ$ probabilistic methods do this similarly, and thus we only list the Sig-Rot equations and leave out the Sig-Trans equations for the rest of the variations in Table I. However, given the Sig-Rot equations, it is non-trivial to solve for R_X, R_Y or R_Z due to the quadratic terms in Eq. 24. One can employ an exhaustive optimization approach on three Sig-Rot equations (e.g., No. 1,3,6 in Table I) to solve for R_X, R_Y and R_Z simultaneously, but that requires one or several good initial guesses to reach the global minimum. We focus on designing methods that do not require initial guesses at all and it turns out that this is achieved by employing the physical properties of the robotic systems as described in the next paragraph.

Note that for the three types of robotic systems described in Fig. 1, Fig. 2 and Fig. 3, different types of constraints can be applied onto the datasets $\{A_i\}$, $\{B_i\}$ and $\{C_i\}$. For the multi-mobile robotic system, any two robot agents can remain static with the third agent moving freely. Or equivalently, any one of A, B and C can be fixed without fixing the other two. For the dual-arm and serial-parallel robotic systems, only A or C can be fixed without fixing the other two. This is because B describes the transformation between the marker frame and the camera frame, while A and C are solely determined using the forward kinematics of the robots. Hence it is very difficult to keep B constant while varying A and C. Hence in the next part, we present the frameworks for solving the calibration problem for each of these two types of systems.

B. Two Frameworks for AXB = YCZ Calibration

Before presenting the two frameworks, we present Theorem 1 to simplify the computation of the mean and covariance of H^{-1}.

Theorem 1 *If the mean and covariance are M and Σ for a PDF $f(H)$, then the mean and covariance for $f(H^{-1})$ are M^{-1} and $Ad(M)\Sigma Ad^T(M)$ respectively.*

Please refer to the appendix for the proof. Theorem 1 provides a simple way to calculate the mean and covariance of $f(H^{-1})$, which is very useful due to the frequent calculations of PDFs on the inverses of $\{A, B, C\}$. Another equation extracted from Eq. (59) is

$$\Sigma_{K^{-1}} = R_K \Sigma_K R_K^T. \tag{26}$$

which is useful when converting the Sig-Rot equations into the simplified versions shown in the last column of Table I.

1) Framework 1: For the dual-arm and serial-parallel systems, we show that X, Y and Z can be recovered without a priori knowledge of the correspondence between the data. This is achieved by fixing A and C to give datasets I and II respectively. When A is fixed, or equivalently $A = A_I$, datasets $\{B_{Ii}\}$ and $\{C_{Ij}\}$ can be measured where $i, j = 1, \cdots, n$. In addition, with the zero covariance constraints, $\Sigma_{A_I} = \mathbb{O}$ and $\Sigma_{A_I^{-1}} = R_{A_I}\Sigma_A R_{A_I}^T = \mathbb{O}$, we can simplify Eq. (24) to the form

$$\Sigma_{B_I}^1 = R_Z^T \Sigma_{C_I}^1 R_Z. \tag{27}$$

However, note that the zero constraint on Σ_{A_I} applies to neither Rep.3 nor Rep.6, where Rep.3 and Rep.6 denote the No.3 and No.6 Representation equations in Table I respectively. When A is fixed to A_I, the right hand side of Rep.6, namely $Y^{-1}A_I X$, becomes a single "point" on $SE(3)$, whereas both C_{Ii} and B_{Ij}^{-1} are PDFs on $SE(3)$. The corresponding convolution equation of Rep.6 becomes

$$(f_{C_I} * \delta_Z * f_{B_I^{-1}})(H) \approx (\delta_{Y^{-1}} * \delta_{A_I} * \delta_X)(H). \tag{28}$$

which does not hold because the convolution of PDFs is a general PDF instead of a Dirac delta function. Therefore, the

No.	Representation	Sig-Rot	Fixing	Simplified Sig-Rot
1	$AXB = YCZ$	$R_B^T R_X^T \Sigma_A^1 R_X R_B + \Sigma_B^1 = R_Z^T \Sigma_C^1 R_Z$	A	$\Sigma_B^1 = R_Z^T \Sigma_C^1 R_Z$
2	$A^{-1}YC = XBZ^{-1}$	$R_C^T R_Y^T \Sigma_{A^{-1}}^1 R_Y R_C + \Sigma_C^1 = R_{Z^{-1}}^T \Sigma_B^1 R_{Z^{-1}}$		
3	$BZ^{-1}C^{-1} = X^{-1}A^{-1}Y$	$R_{C^{-1}}^T R_{Z^{-1}}^T \Sigma_B^1 R_{Z^{-1}} R_{C^{-1}} + \Sigma_{C^{-1}}^1 = R_Y^T \Sigma_{A^{-1}}^1 R_Y$	B	$R_C \Sigma_C^1 R_C^T = R_Y^T R_A \Sigma_A^1 R_A^T R_Y$
4	$B^{-1}X^{-1}A^{-1} = Z^{-1}C^{-1}Y^{-1}$	$R_{A^{-1}}^T R_{X^{-1}}^T \Sigma_{B^{-1}}^1 R_{X^{-1}} R_{A^{-1}} + \Sigma_{A^{-1}}^1 = R_{Y^{-1}}^T \Sigma_{C^{-1}}^1 R_{Y^{-1}}$		
5	$C^{-1}Y^{-1}A = ZB^{-1}X^{-1}$	$R_A^T R_{Y^{-1}}^T \Sigma_{C^{-1}}^1 R_{Y^{-1}} R_A + \Sigma_A^1 = R_{X^{-1}}^T \Sigma_{B^{-1}}^1 R_{X^{-1}}$	C	$R_B \Sigma_B^1 R_B^T = R_X^T \Sigma_A^1 R_X$
6	$CZB^{-1} = Y^{-1}AX$	$R_{B^{-1}}^T R_Z^T \Sigma_C^1 R_Z R_{B^{-1}} + \Sigma_{B^{-1}}^1 = R_X^T \Sigma_A^1 R_X$		

TABLE I: The simplified Sig-Rot equations after fixing A, B or C

underlying constraint of every convolution equation is that there should be at least one non-trivial PDF on both sides of the equation, and we call it the balanced-PDF constraint. The zero covariance constraint can only be applied to the Sig-Rot equation whose corresponding convolution equation satisfies the balanced-PDF constraint.

As shown in [2], Σ_B^1 and Σ_C^1 have the same eigenvalues due to the fact that Eq. (27) is a similarity transformation between Σ_B^1 and Σ_C^1. Calculate the eigendecomposition of Σ_B and Σ_C as $\Sigma_B^1 = Q_B \Lambda Q_B^T$ and $\Sigma_C^1 = Q_C \Lambda Q_C^T$ where Λ denotes the diagonal matrix. Substitute these two equations into Eq. (27), and we have

$$\Lambda = \underbrace{Q_B^T R_Z^T Q_C}_{\mathcal{Q}} \Lambda Q_C^T R_Z Q_B = \mathcal{Q} \Lambda \mathcal{Q}^T. \tag{29}$$

According to [2], the special structure of Eq. (29) gives four solutions for $\mathcal{Q}$. Thus, we also get four candidates of R_Z as:

$$\boxed{R_Z = Q_{C_I} \mathcal{Q} Q_{B_I}^T.} \tag{30}$$

For the translation part t_Z, Eq. (25) can be simplified as

$$\Sigma_{B_I}^2 = R_Z^T \Sigma_{C_I}^1 R_Z U_Z^T + R_Z^T \Sigma_{C_I}^2 R_Z \tag{31}$$

and $t_Z = U_Z^\vee$ can be solved directly.

Similarly, when fixing $C \equiv C_{II}$, $\Sigma_{C_{II}} = \Sigma_{C_{II}^{-1}} = \mathbb{O}$, the Sig-Rot equation for Rep.6 (denoted as Sig-Rot.6) becomes

$$\Sigma_{B_{II}^{-1}}^1 = R_X^T \Sigma_{A_{II}}^1 R_X. \tag{32}$$

Recall that this leads to an equation with structure similar to Eq. (29) and so $\mathcal{Q}$ has four possibilities, and the four candidates of R_X can be calculated as

$$\boxed{R_X = Q_{A_{II}} \mathcal{Q} Q_{B_{II}^{-1}}^T} \tag{33}$$

There are two possible methods to recover Y. One method is to apply $\Sigma_C^1 = \mathbb{O}$ to Sig-Rot.2 to get

$$R_C^T R_Y^T \Sigma_{A^{-1}}^1 R_Y R_C = R_{Z^{-1}}^T \Sigma_B^1 R_{Z^{-1}}, \tag{34}$$

and hence we obtain a total of sixteen candidates of R_Y that are based on the candidates of $\mathcal{Q}$ and R_Z:

$$R_Y = Q_{A^{-1}} \mathcal{Q} Q_B^T R_Z^T R_C^T. \tag{35}$$

The other method is to employ the mean equations to recover Y using the candidates of X and Z as

$$\boxed{Y = A_I X M_{B_I} Z^{-1} M_{C_I}^{-1}} \tag{36}$$

and

$$\boxed{Y = M_{A_{II}} X M_{B_{II}} Z^{-1} C_{II}^{-1}} \tag{37}$$

Hence the second approach gives a total of $16{+}16 = 32$ candidates of Y. When numerically simulating the two approaches above, the second approach is better in terms of generating candidates of Y that are closer to the ground truth, whereas the first one is more likely to result in candidates far from the true Y.

The solution for t_Z and t_X becomes trivial once R_Z and R_X are known. Using the second approach to compute Y, we will have a total of $4 \times 4 \times 32 = 512$ combinations of $\{X, Y, Z\}$. In order to filter out the best combination among the 512 choices, the two datasets can be used to minimize an objective function. For simplicity, let $M_{L_I} = A_I X_i M_{B_I}$, $M_{R_I} = Y_j M_{C_I} Z_k$, $M_{L_{II}} = M_{A_{II}} X_i M_{B_{II}}$ and $M_{R_{II}} = Y_j C_{II} Z_k$.

It turns out that the objective function is critical in getting an optimal X, Y, Z consistently out of the possible 512 candidates. We tried a few functions and found that this function

$$\begin{aligned} \min & || \log^\vee (R_{M_{L_I}}^T R_{M_{R_I}}) ||_2 + || \log^\vee (R_{M_{L_{II}}}^T R_{M_{R_{II}}}) ||_2 \\ & w \cdot ||t_{M_{L_I}} - t_{M_{R_I}}||_2 + w \cdot ||t_{M_{L_{II}}} - t_{M_{R_{II}}}||_2 \end{aligned} \tag{38}$$

where $i = 1, \ldots, 4$, $j = 1, \ldots, 4, k = 1, \ldots, 32$ has the highest success rate of picking the optimal X, Y, Z. Here w is the weighting factor and can be varied depending on the precision requirement on rotation and translation. Different X, Y, Z will be selected given different w, and we settled on $w = 1.5$ for the simulation.

2) Framework 2: For the multi-robot hand-eye calibration problem, a less restrictive approach exists to solve for X, Y and Z. In addition to fixing A or C, we can also fix B, and this will produce three datasets that are labeled as follows.

Dataset I: $A = A_I$ with $\{B_{Ii}\}$ and $\{C_{Ij}\}$

$$\Sigma_B^1 = R_Z^T \Sigma_C^1 R_Z. \tag{39}$$

Dataset II: $B = B_{II}$ with $\{A_{IIi}\}$ and $\{C_{IIj}\}$

$$\Sigma_{C^{-1}}^1 = R_Y^T \Sigma_{A^{-1}}^1 R_Y. \tag{40}$$

Dataset III: $C = C_{III}$ with $\{A_{IIIi}\}$ and $\{B_{IIIj}\}$

$$\Sigma^1_{B^{-1}} = R_X^T \Sigma^1_A R_X. \tag{41}$$

Under this situation, X, Y and Z are solved independently and there are a total of $4 \times 4 \times 4 = 64$ combinations of solutions. By letting $M_{L_{III}} = M_{A_{III}} X_i M_{B_{III}}$ and $M_{R_{III}} = Y_j C_{III} Z_k$, we can form the following objective function using all 3 datasets:

$$\begin{aligned} \min & || \log^\vee (R^T_{M_{L_I}} R_{M_{R_I}})||_2 + || \log^\vee (R^T_{M_{L_{II}}} R_{M_{R_{II}}})||_2 \\ & || \log^\vee (R^T_{M_{L_{III}}} R_{M_{R_{III}}})||_2 + w \cdot ||t_{M_{L_I}} - t_{M_{R_I}}||_2 + \\ & w \cdot ||t_{M_{L_{II}}} - t_{M_{R_{II}}}||_2 + w \cdot ||t_{M_{L_{III}}} - t_{M_{R_{III}}}||_2 \\ \text{where } & i = 1, \cdots, 4, \ j = 1, \cdots, 4 \text{ and } k = 1, \cdots, 4. \end{aligned} \tag{42}$$

IV. Numerical Simulation

In this section, we compared our probabilistic approaches numerically with the existing methods in the literature. For convenience, we called the probabilistic methods presented in Framework 1 and Framework 2, *Prob1* and *Prob2* respectively. In [23], two approaches were proposed for solving the $AXB = YCZ$ problem: one is called the *DK* method while the other is the *PN* method. In [20], a simultaneous $AXB = YCZ$ solver was introduced and we call it *Wang* in this paper. Note that all of the three methods in the literature require a priori knowledge of the exact correspondence between the datasets $\{A_i\}$, $\{B_i\}$ and $\{C_i\}$, and in this section we refer to them as the "traditional methods". We performed numerical simulations on both the traditional and probabilistic methods to show that: 1) probabilistic approaches showed superior performance when dealing with data that has little or no correspondence compared to traditional solvers; 2) *Prob2* performed better than *Prob1* when the former had complete datasets.

There are several things to pay attention to when comparing the probabilistic approaches with the traditional methods. Firstly, *PN* is an unconstrained nonlinear optimization algorithm which requires multiple initial guesses of X, Y and Z to achieve an almost global minimum solution. Secondly, *Wang* is a least-squares-based search algorithm that requires good initial guesses of at least two of R_X, R_Y and R_Z. Thirdly, both of them are simultaneous approaches meaning that none of A, B or C needs to be fixed during the calibration process. Lastly, DK is a separable method requiring A or C to be fixed during the calibration process. However, no initial guesses are needed to obtain the final result.

A. Data Generation and Error Metrics

In order to compare all of the five $AXB = YCZ$ solvers together, we generated the simulated datasets as follows. First, we fixed A such that $A = A_I$, and $\{B_{Ii}\}$ are given by

$$B_{Ii} = \exp(\hat{\delta}_i) B_{I0} \tag{43a}$$

$$\delta_i \in \mathcal{N}(\mathbf{0}; \Sigma) \subset \mathbb{R}^6 \tag{43b}$$

where the mean $\mu = \mathbf{0} \in se(3)$, the covariance matrix $\Sigma = \sigma_{\text{data}} \mathbb{I}_6 \in \mathbb{R}^{6\times 6}$ and $i = 1, 2, \ldots, 100$. The hat operator $\hat{}$ converts a 6 by 1 vector into its corresponding Lie algebra in $se(3)$. Given the ground truth of X, Y and Z, $\{C_{Ii}\}$ is generated by

$$C_{Ii} = Y^{-1} A_I X B_{Ii} Z^{-1}, \tag{44}$$

and we call this dataset I.

Then, we generated dataset II where we fixed C such that $C = C_{II}$, and generated B_{IIi} and A_{IIi} in a similar fashion:

$$B_{IIi} = \exp(\hat{\delta}_i) B_{II0} \tag{45a}$$

$$A_{IIi} = Y C_{II} Z B^{-1}_{IIi} X^{-1} \tag{45b}$$

Lastly, dataset III was obtained by fixing B such that $B = B_{III}$, and $\{A_{IIIi}\}$, $\{C_{IIIi}\}$ were given by

$$A_{IIIi} = \exp(\hat{\delta}_i) A_{III0} \tag{46a}$$

$$C_{IIIi} = Y^{-1} A_{III} X B_{IIi} Z^{-1}. \tag{46b}$$

In each dataset, the number of measurement data for A, B, C is 100, i.e. $i = 1, \ldots, 100$. Note that there were a total of three datasets but only the first two could be applied on *DK* and *Prob1* methods, but all three sets could be used by *PN*, *Wang* and *Prob2* methods. In order to compare the methods, the datasets being passed into each method are indicated by checkmarks in Table II. The recovered X, Y and Z were compared with the actual transformations using the following metrics for the errors in rotation and translation:

$$Error(R_H) = \| \log^\vee (R^T_{H_{\text{solved}}} R_{H_{\text{true}}}) \| \tag{47a}$$

$$Error(t_H) = \| t_{H_{\text{solved}}} - t_{H_{\text{true}}} \| \ / \ \| t_{H_{\text{true}}} \| \tag{47b}$$

where $H = X, Y, Z$.

	Dataset	*Prob1*	*Prob2*	*Wang*	*PN*	*DK*
I	$A_I, \{B_{Ii}\}, \{C_{Ii}\}$	✓	✓	✓	✓	✓
II	$C_{II}, \{B_{IIi}\}, \{A_{IIi}\}$	✓	✓	✓	✓	✓
III	$B_{III}, \{A_{IIIi}\}, \{C_{IIIi}\}$	×	✓	✓	✓	×

TABLE II: Datasets used on each method

B. Simulation and Discussion

To compare all the five algorithms comprehensively, we performed numerical simulations by varying

1) the scrambling rate r,
2) standard deviation σ_{data} for generating the measurement data,
3) noise level σ_{noise}.

For each set of conditions, we ran 10 trials and plotted the average error of the computed X, Y, Z from the true values. For experiments (2) and (3) the range of the errors were very big across all the methods. Hence we used the logarithm scale for the vertical axis in Fig. (5), Fig. (6) and Fig. (7).

First, given the three sets of $\{A\}$, $\{B\}$ and $\{C\}$, we scrambled B_{Ii}, A_{IIi}, C_{IIIi} up to a certain percentage r where $r = 0\%, 20\%, 40\%, 60\%, 80\%, 100\%$. We set $\sigma_{\text{data}} = 0.02$ to generate the original datasets A, B and C. 10 trials were run for each algorithm at each scrambling rate r, and the average

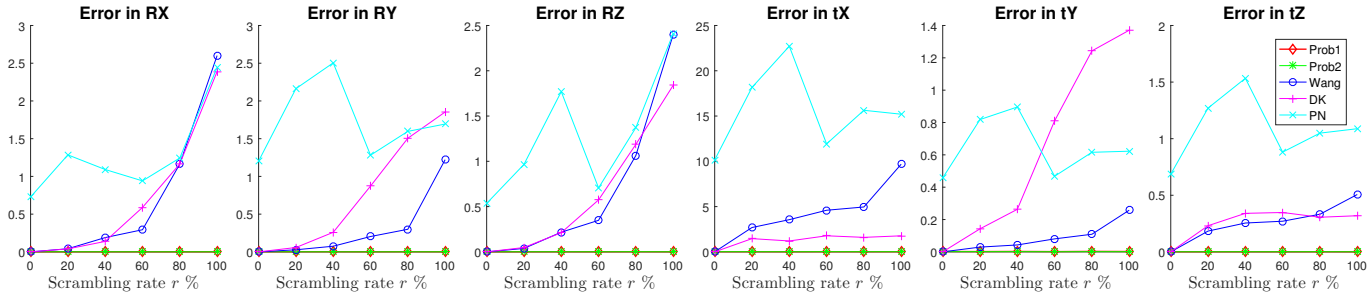

Fig. 4: Rotation/Translation Errors in X, Y, Z v.s. scrambling rate for 10 trials and 100 measurements

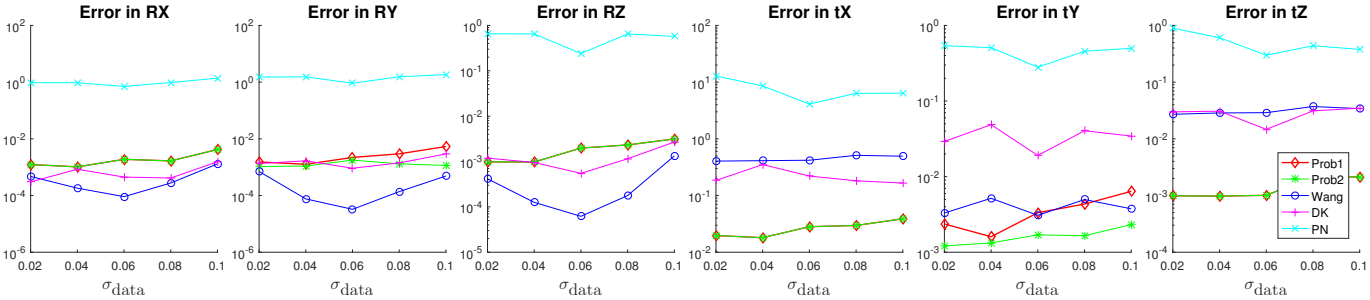

Fig. 5: Rotation/Translation errors v.s. standard deviation of measurement data for $r = 1\%$ and $\sigma_{\text{noise}} = 0$

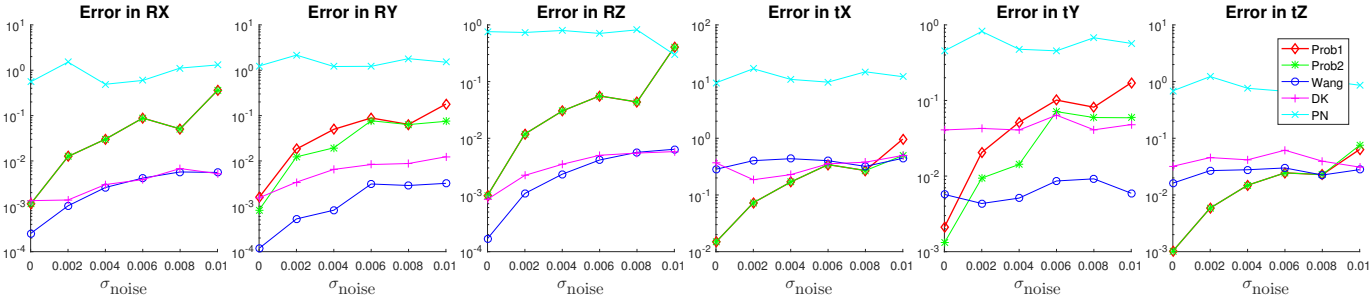

Fig. 6: Rotation/Translation errors v.s. standard deviation of noise applied to the data for $r = 1\%$ and $\sigma_{\text{data}} = 0.02$

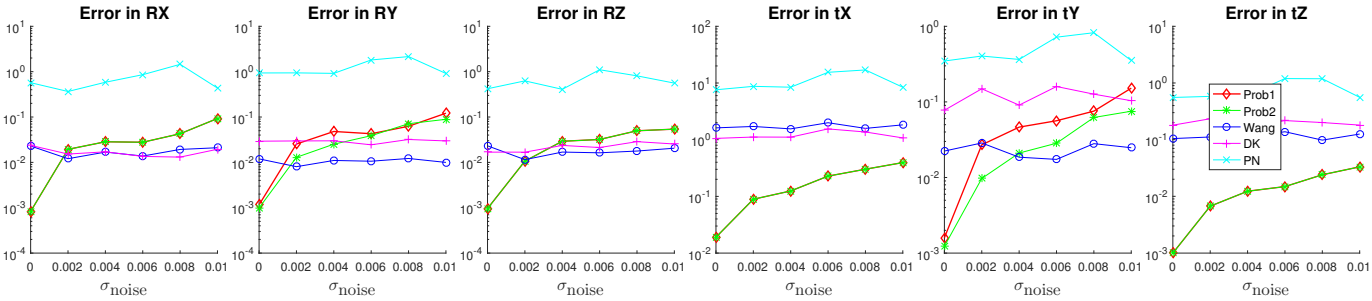

Fig. 7: Rotation/Translation errors v.s. standard deviation of noise applied to the data for $r = 10\%$ and $\sigma_{\text{data}} = 0.02$

errors in rotation and translation were plotted as in Fig. (4). It can be seen that the rotation and translation errors of both *Prob1* and *Prob2* remain close to zero despite the scrambling rate r increasing, while the errors of *DK*, *PN* and *Wang* either diverged quickly or blew up in the beginning. This showed the outstanding performance of the probabilistic approaches when dealing with data streams that had missing correspondence information. In addition, no initial estimates of any kind were needed to calculate X, Y and Z.

Next, we varied the datasets with different values of σ_{data} where $\sigma_{\text{data}} = \{0.02, 0.04, 0.06, 0.08, 0.1\}$ and $r = 1\%$. As shown in Fig. (5), as the standard deviation σ_{data} increased, both the rotation and translation errors increased. This was consistent with the assumption on the datasets that they should be "highly focused". Moreover, *Prob2* gave smaller rotation and translation errors compared to *Prob1*, when all three datasets were available. This meant that although *Prob1* can be applied to a broader scope of robotic systems, *Prob2* is

preferable if the system allowed the acquisition of complete datasets. This is important because candidates of Y can affect the picking of both X and Z. If no Y is close to its ground truth, it is possible to pick the wrong X and Z even when there are some candidates very close to their ground truths. Besides, the performance of the probabilistic methods in general are comparable to or better than the traditional methods even when the scrambling rate is as low as 1%.

In the real world, data gathered from experiments are usually noisy, and it is interesting to see how the five algorithms perform with noisy and scrambled data. In Fig. (6) and Fig. (7), we fixed the standard deviation for generating the datasets as $\sigma_{\text{data}} = 0.02$. For a homogeneous matrix H, we apply noise with zero mean and standard deviation $\sigma_{\text{noise}} = \{0, 0.002, 0.004, 0.006, 0.008, 0.01\}$ to get a noisy $H_{\text{noise}} = H\exp(\hat{\delta})$, $\delta \in \mathcal{N}(\mathbf{0}; \Sigma)$, where the covariance matrix $\Sigma = \sigma_{\text{noise}}\mathbb{I}_6 \in \mathbb{R}^{6\times 6}$. The scrambling rate in Fig. (6) is $r = 1\%$ and the scrambling rate in Fig. (7) is $r = 10\%$. There are several observations from these two figures.

1) Probabilistic methods deteriorate relatively faster than the traditional methods when the scrambling rate is very low, in this case $r = 1\%$.
2) The probabilistic methods become closer or much better than the traditional methods when the scrambling rate increases from 1% to 10%, despite the effects of noise.
3) For traditional methods, the scrambling rate was the dominant factor on the errors of the solved X, Y and Z when it is large enough. As in Fig. (7), when $r = 10\%$, the performance of the traditional methods only fluctuated within a small range despite the increasing noise.

V. Conclusion and Future Work

Motivated by problems that arise in multi-robot systems, in this paper we proposed two probabilistic approaches to solve the $AXB = YCZ$ calibration problem for the case where partial or all correspondence information between the datasets was lost. Numerical simulations were performed to show the outstanding performance of the probabilistic approaches over the traditional $AXB = YCZ$ solvers that demand exact correspondence among the datasets. In addition, the probabilistic approaches did not require initial estimates which made the calibration process easier. We compared the performance between the two probabilistic approaches and showed that given complete datasets, *Prob2* gave better R_Y and t_Y. However, *Prob1* required fewer datasets and had wider applications. Possible future work includes deriving a simultaneous probabilistic approach that can deal with scrambled data obtained without fixing any degrees of freedom in the system. It is also worthwhile to check the performance of the current probabilistic approaches in real world applications.

Appendix

A. Proof for Theorem 1

Proof: Let $f'(H) = f(H^{-1})$ whose mean and covariance are M' and Σ' satisfying the following equations

$$\int_{SE(3)} \log(M'^{-1}H) f'(H) dH = \mathbb{O} \tag{48}$$

and

$$\Sigma' = \int_{SE(3)} \log^{\vee}(M'^{-1}H)[\log^{\vee}(M'^{-1}H)]^T f'(H) dH. \tag{49}$$

After a simple substitution, Eq.(48) becomes

$$\int_{SE(3)} \log(M'^{-1}H) f(H^{-1}) dH = \mathbb{O}. \tag{50}$$

Next, set $K = H^{-1}$ and use the invariance of integration under inversion, Eq. (50) becomes:

$$\int_{SE(3)} \log(M'^{-1}K^{-1}) f(K) dK = \mathbb{O}. \tag{51}$$

Premultiply M' and postmultiply M'^{-1} on both sides of the equation to get

$$\int_{SE(3)} \log(K^{-1}M'^{-1}) f(K) dK = \mathbb{O} \tag{52}$$

by using the property

$$H_1(\log H_2)H_1^{-1} = \log(H_1 H_2 H_1^{-1}). \tag{53}$$

Eq.(52) can be further written as

$$\int_{SE(3)} \log(M'K) f(K) dK = \mathbb{O}, \tag{54}$$

given $\log(H^{-1}) = -\log H$. This shows that $M' = M^{-1}$.

By definition, covariance Σ' will be

$$\Sigma' = \int_{SE(3)} \log^{\vee}(M'^{-1}H)[\log^{\vee}(M'^{-1}H)]^T f(H^{-1}) dH \tag{55}$$

which becomes

$$\Sigma' = \int_{SE(3)} \log^{\vee}(MK^{-1})[\log^{\vee}(MK^{-1})]^T f(K) dK \tag{56}$$

under a change of variables and substitution of $M' = M^{-1}$. Knowing that

$$\begin{aligned} Ad(H_1)\log^{\vee}(H_2) &= \log^{\vee}(H_1 H_2 H_1^{-1}) \\ \log^{\vee}(K^{-1}M) &= -\log^{\vee}(M^{-1}K) \end{aligned} \tag{57}$$

$$\begin{aligned} &Ad(M^{-1})\Sigma' Ad^T(M^{-1}) = \\ &\int_{SE(3)} \log^{\vee}(K^{-1}M)[\log^{\vee}(K^{-1}M)]^T f(K) dK \end{aligned} \tag{58}$$

so that

$$Ad(M^{-1})\Sigma' Ad^T(M^{-1}) = \Sigma \tag{59}$$

which, after inversion of the *Ad* matrices, completes the proof. ■

References

[1] F. Aalamifar, D. Jiang, H.K. Zhang, A. Cheng, X. Guo, R. Khurana, I. Iordachita, and E. M. Boctor. Co-robotic ultrasound tomography: dual arm setup and error analysis. In *SPIE Medical Imaging*, pages 94190N–94190N. International Society for Optics and Photonics, 2015.

[2] M. K. Ackerman and G. S. Chirikjian. A probabilistic solution to the AX = XB problem: Sensor calibration without correspondence. In *Geometric Science of Information*, pages 693–701. Springer, 2013.

[3] M. K. Ackerman, A. Cheng, E. M. Boctor, and G.S. Chirikjian. Online ultrasound sensor calibration using gradient descent on the euclidean group. In *IEEE International Conference on Robotics and Automation (ICRA)*, pages 4900–4905. IEEE, 2014.

[4] M. K. Ackerman, A. Cheng, and G.S. Chirikjian. An information-theoretic approach to the correspondence-free AX = XB sensor calibration problem. In *IEEE International Conference on Robotics and Automation (ICRA)*, pages 4893–4899. IEEE, 2014.

[5] G. S. Chirikjian. *Stochastic Models, Information Theory, and Lie Groups, Volume 2: Analytic Methods and Modern Applications*, volume 2. Springer Science & Business Media, 2011.

[6] G.S. Chirikjian and A.B. Kyatkin. *Harmonic Analysis for Engineers and Applied Scientists*. Dover, 2016.

[7] K. Daniilidis. Hand-eye calibration using dual quaternions. *The International Journal of Robotics Research*, 18(3):286–298, 1999.

[8] J. D. Davis, Y. Sevimli, M. K. Ackerman, and G. S. Chirikjian. A robot capable of autonomous robotic team repair: The Hex-DMR II system. In *Advances in Reconfigurable Mechanisms and Robots II*, pages 619–631. Springer, 2016.

[9] F. Ernst, L. Richter, L. Matthäus, V. Martens, R. Bruder, A. Schlaefer, and A. Schweikard. Non-orthogonal tool/flange and robot/world calibration. *The International Journal of Medical Robotics and Computer Assisted Surgery*, 8(4):407–420, 2012.

[10] I. Fassi and G. Legnani. Hand to sensor calibration: A geometrical interpretation of the matrix equation AX = XB. *Journal of Robotic Systems*, 22(9):497–506, 2005.

[11] J. Ha, D. Kang, and F. C. Park. A stochastic global optimization algorithm for the two-frame sensor calibration problem. *IEEE Transactions on Industrial Electronics*, 2016.

[12] R.L. Hirsh, G.N. DeSouza, and A.C. Kak. An iterative approach to the hand-eye and base-world calibration problem. In *IEEE International Conference on Robotics and Automation (ICRA)*, volume 3, pages 2171–2176. IEEE, 2001.

[13] R. Horaud and F. Dornaika. Hand-eye calibration. *The International Journal of Robotics Research*, 14(3):195–210, 1995.

[14] A. Li, L. Wang, and D. Wu. Simultaneous robot-world and hand-eye calibration using dual-quaternions and Kronecker product. *The International Journal of Physical Sciences*, 5(10):1530–1536, 2010.

[15] H. Li, Q. Ma, T. Wang, and G.S. Chirikjian. Simultaneous hand-eye and robot-world calibration by solving the $AX = YB$ problem without correspondence. *IEEE Robotics and Automation Letters (RA-L)*, 2016.

[16] F.C. Park and B.J. Martin. Robot sensor calibration: solving AX = XB on the euclidean group. *IEEE Transactions on Robotics and Automation*, 10(5), 1994.

[17] M. Shah. Solving the robot-world/hand-eye calibration problem using the Kronecker product. *Journal of Mechanisms and Robotics*, 5(3):031007, 2013.

[18] Y.C. Shiu and S. Ahmad. Calibration of wrist-mounted robotic sensors by solving homogeneous transform equations of the form AX = XB. *IEEE Transactions on Robotics and Automation*, 5(1):16–29, 1989.

[19] R.Y. Tsai and R.K. Lenz. A new technique for fully autonomous and efficient 3d robotics hand/eye calibration. *IEEE Transactions on Robotics and Automation*, 5 (3):345–358, 1989.

[20] J. Wang, L. Wu, M. Q-H Meng, and H. Ren. Towards simultaneous coordinate calibrations for cooperative multiple robots. In *IEEE/RSJ International Conference on Intelligent Robots and Systems (IROS)*, pages 410–415. IEEE, 2014.

[21] Y. Wang and G.S. Chirikjian. Nonparametric second-order theory of error propagation on motion groups. *The International Journal of Robotics Research*, 27(11-12): 1258–1273, 2008.

[22] L. Wu, J. Wang, L. Qi, K. Wu, H. Ren, and M. Q. H. Meng. Simultaneous hand-eye, tool-flange, and robot-robot calibration for comanipulation by solving the $AXB = YCZ$ problem. *IEEE Transactions on Robotics*, 32(2):413–428, April 2016. ISSN 1552-3098. doi: 10.1109/TRO.2016.2530079.

[23] S.J. Yan, S.K. Ong, and A.Y.C. Nee. Registration of a hybrid robot using the degradation-Kronecker method and a purely nonlinear method. *Robotica*, pages 1–12, 12 2015.

[24] Z. Zhao. Hand-eye calibration using convex optimization. In *IEEE International Conference on Robotics and Automation (ICRA)*, pages 2947–2952. IEEE, 2011.

[25] H. Zhuang, Z.S. Roth, and R. Sudhakar. Simultaneous robot/world and tool/flange calibration by solving homogeneous transformation equations of the form AX = YB. *IEEE Transactions on Robotics and Automation*, 10(4): 549–554, 1994.